Complexity in "Simple" Electrolyte Solutions: Ion Pairing in $MgSO_4$(aq)

Richard Buchner*

Institut für Physikalische und Theoretische Chemie, Universität Regensburg, D-93040 Regensburg, Germany

Ting Chen and Glenn Hefter*

Chemistry Department & A. J. Parker Cooperative Research Centre for Hydrometallurgy, Murdoch University, Murdoch, WA 6150, Australia

Received: April 3, 2003; In Final Form: November 21, 2003

A detailed investigation of aqueous solutions of $MgSO_4$ has been made by dielectric relaxation spectroscopy over a wide range of frequencies ($0.2 \leq \nu/\text{GHz} \leq 89$) and concentrations ($0.017 \leq c/\text{M} \leq 2.24$). Detailed analysis of the spectra shows conclusively, as has long been inferred from ultrasonic absorption studies, the simultaneous presence of double solvent separated (2SIP), solvent-shared (SIP), and contact (CIP) ion pairs. The constants derived for the stepwise formation of each ion pair type and for the overall association are in excellent agreement with literature estimates based on other kinds of measurements. In addition, evidence has been obtained for the existence of a triple ion, $Mg_2SO_4^{2+}$(aq), or possibly a more aggregated species, at high electrolyte concentrations ($c > 1$ M). Support for the presence of CIPs, SIPs, and the triple ion is provided by Raman spectroscopy. The implications of the present findings for quantitative models of the thermodynamic behavior of higher-valent electrolytes are briefly discussed.

1. Introduction

Divalent metal sulfates are archetypal 2:2 salts that have played a central role in defining the characteristics of higher-valent electrolyte solutions. Such solutions have been widely used to test various theories of strong electrolyte behavior[1−4] and to develop models of ion association in solution;[5−7] they are also of considerable practical importance.[8−10] However, despite some progress,[2,11] theoretical description of divalent metal sulfate solutions has proven to be difficult. Undoubtedly, a major reason for this is the difficulty of accounting, in a physically meaningful manner, for the strong interactions that occur in such solutions.

Evidence from a variety of techniques[12−17] supports the notion that divalent metal sulfate solutions are significantly associated. In particular, using ultrasonic relaxation techniques, Eigen and others[5−7] have established the presence of three *equilibria* (as distinct from *species*) in such solutions. These observations were used to formulate a widely applied[18] three-step mechanism (Scheme I) of ion association:

$$\underset{\text{free ions}}{M^{m+}(aq) + L^{n-}(aq)} \overset{K_1}{\leftrightarrow} \underset{\text{2SIP}}{[M^{m+}(OH_2)(OH_2)L^{n-}](aq)} \overset{K_2}{\leftrightarrow} \underset{\text{SIP}}{[M^{m+}(OH_2)L^{n-}](aq)} \overset{K_3}{\leftrightarrow} \underset{\text{CIP}}{[ML]^{(m-n)+}(aq)} \quad \text{(I)}$$

where free hydrated ions initially combine to form double solvent separated or outer-outer-sphere ion pairs (2SIP), in which the hydration sheath of each ion remains essentially intact. This step is followed by a loss of water molecules to form, successively, solvent-shared or outer-sphere (SIP) and contact or inner-sphere (CIP) ion pairs.

Unfortunately, agreement about the *extent* of ion pairing in divalent metal sulfate solutions is poor, with reported association constants varying[12,19] from ca. 0−200 L mol^{-1}. These factors have led many researchers[3,12,19] to continue to prefer theoretical models that take no account of speciation, with at least one experienced writer suggesting that "there is no clear evidence that [divalent metal sulfate solutions] associate" (ref 19, p 813). Clearly, there is a need to better define the speciation of these more-or-less strong electrolyte solutions.

Dielectric relaxation spectroscopy (DRS), which probes a sample's response to an applied electromagnetic field as a function of its frequency, is a powerful tool for the investigation of electrolyte solutions.[20] In particular, because the dielectric response is sensitive to the square of the dipole moment of any dipolar species present, DRS is able, at least in principle, not only to detect the presence of small concentrations of ion pairs but also to distinguish between the various types.[21] Uniquely among spectroscopic techniques, DRS shows a sensitivity in the order 2SIP > SIP > CIP.[21]

Several DRS studies of divalent metal sulfate solutions have been reported[22−24] but because of then-existing technological restrictions, only limited information about the ion pairing was obtained. Advances in DR instrumentation[20,25] and processing techniques[25,26] make timely a thorough reinvestigation of these solutions. The DRS data have been supplemented with some carefully targeted Raman spectroscopic measurements.[27] Magnesium sulfate was chosen as the initial part of a systematic investigation of the divalent metal sulfate solutions[27] because, in addition to its intrinsic importance,[8−10,28,29] it does not hydrolyze significantly at 25 °C and high-quality Raman spectroscopic[16,17] and conductance[14] studies are available for comparison.

2. Experimental Section

All solutions were prepared volumetrically, without buoyancy corrections, using calibrated A-grade glassware and high-purity

* To whom correspondence should be addressed. For R.B.: (e-mail) Richard.Buchner@chemie.uni-regensburg.de. For G.H.: (e-mail) hefter@chem.murdoch.edu.au.

10.1021/jp034870p CCC: $27.50
Published on Web 01/23/2004

water (Millipore Milli-Q systems). Concentrations are expressed in moles of solute per liter of solution (M) throughout. Samples of $MgSO_4 \cdot 7H_2O$ were either AR grade, 99.8% pure from Ajax Chemicals, Australia (for the measurements at Murdoch University), or pa grade, 99.5% purity from Merck (for the measurements at Regensburg) and were used without further purification. Exact concentrations were determined to ±0.2% by titration against EDTA (BDH, U.K., concentrated volumetric standard). Densities required for the calculation of water concentrations were obtained from the ELDAR database,[30] as were the conductivities of $MgSO_4$(aq) that were used for kinetic depolarization corrections.

Dielectric spectra, consisting of 101 points measured at equally spaced increments of log ν over the frequency range $\nu_{min} \leq \nu/\text{GHz} \leq 20$, were obtained at Murdoch University using a Hewlett-Packard model 85070M dielectric probe system based on a HP 8720D vector network analyzer (VNA) as described previously.[25,26] Temperature was controlled by a Hetofrig (Denmark) circulator-thermostat to 25 ± 0.02 °C with an accuracy of better than 0.05 °C (NIST-traceable). The minimum frequency of investigation, ν_{min}, was dictated by the conductivity contribution to the loss spectrum (see below). As such, ν_{min} varied with concentration but was typically in the range 0.2−0.5 GHz. Spectra were recorded for water and, because of the anticipated complexity of the system, for 18 closely spaced concentrations of $MgSO_4$(aq) over the range $0.017 \leq c/\text{M} \leq 2.24$. All VNA spectra were recorded using at least two independent calibrations (with air, water, and mercury as the standards). Higher frequency data for selected solutions were recorded at Regensburg using two interferometers: A-band ($27 \leq \nu/\text{GHz} \leq 39$) and E-band ($60 \leq \nu/\text{GHz} \leq 89$) at approximately 10 selected frequencies. The operation of these interferometers has been described in detail elsewhere;[31,32] temperature control and accuracy were similar to those at Murdoch. The overall precision of the combined data is difficult to define because it depends on many factors but is of the order of 1−2% of the static permittivity of the sample for both ϵ' and ϵ''. In addition, seven previously published spectra[23,24] obtained by interferometry at Regensburg over the approximate range $1 \leq \nu/\text{GHz} \leq 89$ were incorporated into the database for processing. Note that for these earlier data,[23,24] ν_{min} is substantially higher ($1.0 \leq \nu_{min}/\text{GHz} \leq 1.8$) and the accuracy substantially lower (ca. 5% at $\nu \leq 4$ GHz) than for the present VNA results. This is critical because for the $MgSO_4$(aq) system most of the information about the ion pairs occurs at these lower frequencies. Nevertheless, as has been found previously for other systems,[21,26] all the present and earlier data could be combined seamlessly. No data were omitted except for a few obviously aberrant points in the older spectra at high concentrations and low frequencies. Typical spectra are shown in Figure 1.

Raman spectra were recorded with a Nicolet Magna 850 series II FTIR spectrometer equipped with a Magna Raman module using a Nd:YVO_4 laser operating at 1064 nm with an InGaAs detector. A laser power of 0.67 W, a resolution of 4 cm^{-1}, and 1024 scans were employed throughout. All spectra were measured at 23 ± 2 °C in 5 mm diameter fluorescence-free NMR tubes using 90° scattering geometry. Curve-fitting analysis was performed using the Grams/32 (Galactic Industries Corporation) software.

3. Data Analysis

The complex permittivity ϵ^* ($= \epsilon' - i\epsilon''$) of the samples as a function of frequency consisted of the present VNA and interferometer data supplemented, wherever available, with the previous Regensburg data.[23,24] The combined data were analyzed by simultaneously fitting the in-phase (ϵ', Figure 1a) and out-of-phase (ϵ'', Figure 1b) components to relaxation models based on the sum of n distinguishable dispersion steps:

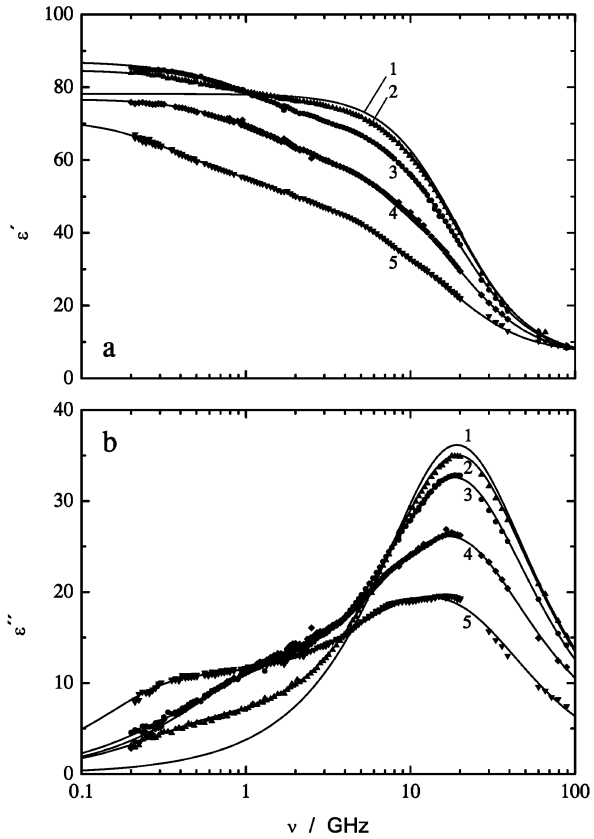

Figure 1. Typical combined DRS spectra for $MgSO_4$(aq) at 25 °C: (a) dielectric permittivity, $\epsilon'(\nu)$, and (b) dielectric loss, $\epsilon''(\nu)$, at $c(MgSO_4)$/M of 0 (1), 0.08 (2), 0.20 (3), 1.2 (4), and 2.24 (5). Solid lines are calculated assuming five Debye processes.

$$\epsilon^*(\nu) = \sum_{j=1}^{n} \frac{\epsilon_j - \epsilon_{j+1}}{[1 + (i2\pi\nu\tau_j)^{1-\alpha_j}]^{\beta_j}} + \epsilon_\infty \qquad (1)$$

The high-frequency permittivity, ϵ_∞, which in principle should contain only contributions from intramolecular polarizability, was used as an adjustable parameter, together with the limiting permittivity ϵ_j, the relaxation time τ_j, and the relaxation-time distribution parameters $0 \leq \alpha_j < 1$ and $0 < \beta_j \leq 1$ of dispersion step j.[33] The static permittivity of the sample is given as $\epsilon = \epsilon_\infty + \sum S_j$ (note that $\epsilon_\infty = \epsilon_{n+1}$) where $S_j = \epsilon_j - \epsilon_{j+1}$ is the amplitude (relaxation strength) of the process j.

Fortunately, as is described below, models such as the Cole−Cole or Cole−Davidson equations that require variable relaxation-time distribution parameters were found to be unable to satisfactorily fit all of the observed data. Only models involving Debye processes, with fixed relaxation-time distribution parameters ($\alpha_j = 0$, $\beta_j = 1$) were successful. Thus, in the final analysis, which yielded the parameters in Table 2, all $\epsilon^*(\nu)$ spectra were fitted to equations of the type

$$\epsilon^*(\nu) = \sum_{j=1}^{n} \frac{\epsilon_j - \epsilon_{j+1}}{1 + i2\pi\nu\tau_j} + \epsilon_\infty \qquad (2)$$

However, before implementation of the final fit, other possible models had to be scrutinized because there are in principle many

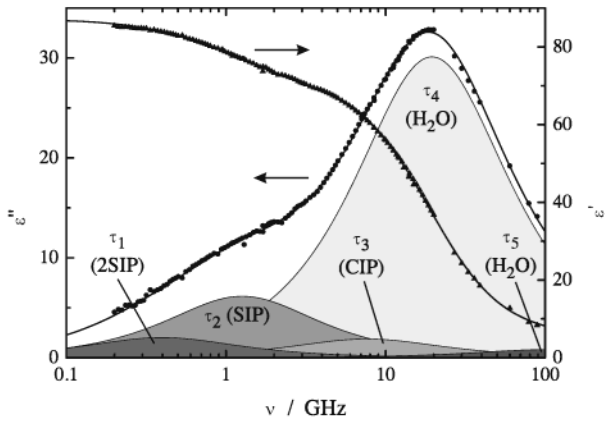

Figure 2. Dielectric permittivity, $\epsilon'(\nu)$, and dielectric loss spectrum, $\epsilon''(\nu)$, of 0.363 M $MgSO_4$(aq) at 25 °C, showing the contributions from the various Debye processes to ϵ''. The solid lines are the sum of the five processes.

(potentially overlapping) relaxation processes that might be occurring in this system and DR spectra are typically very broad. In this context, the fitting of the present spectra[23,24] requires careful consideration. This difficult task is made feasible by two factors. The first is that two complete sets of spectra ($\epsilon'(\nu)$ and $\epsilon''(\nu)$) are fitted simultaneously, and in general, the effects of errors in each are different. For example, at low frequencies, ϵ'' is particularly sensitive to the conductivity correction whereas ϵ' is unaffected. The second is that the processes associated with the solvent are well understood and can be defined with a good level of precision, providing measurements are made (as in the present study) at sufficiently high frequencies (>20 GHz). As discussed in detail by Barthel et al.,[23,34] the selected model must not only show a good fit (low value of the variance σ^2) but also produce spectral parameters (relaxation times and amplitudes) that are physically reasonable for the entire series of experiments and that exhibit (within defined error limits) smooth concentration dependencies. How these problems were addressed is now outlined utilizing the spectrum for 0.363 M $MgSO_4$ (Figure 2) as an example.

The more straightforward, higher frequency data will be considered first. From studies of many simple aqueous electrolyte solutions, the dominant loss peak in Figure 2 at ~8 ps (~20 GHz) is readily assigned to the cooperative relaxation of solvent water molecules. Following the work of Barthel et al.[35] and confirmed by others,[36,37] a small-amplitude faster process, probably associated with the relaxation of "free" water molecules, also needs to be included. This process occurs at the limit of the present spectra (ca. 90 GHz) and cannot always be detected in electrolyte solutions.[38] However, because it was unequivocally detected in $MgSO_4$(aq) at $c \leq 1.1$ M previously[23,24] (and confirmed by the present high-frequency data), it is appropriate to include it at $c = 0.363$ M.

In addition to the solvent-related processes, ϵ'' exhibits a well-developed shoulder at low frequencies (Figure 2), indicating the presence of other processes. Since, a priori, the number of polar components and of *distinguishable* relaxation processes may differ, all conceivable relaxation models with $1 \leq n \leq 6$ were tested (higher values of n produced clear signs of overfitting). The results of these analyses are summarized in Table 1, which lists the fitting parameters for all Debye-process relaxation models that converged for the 0.363 M spectrum using the combined ϵ^* data. Note that at $c = 0.363$ M the data at $\nu > 20$ GHz, which characterize the water contribution, are those of Barthel et al.[23,24] (they were not redetermined at this concentration in the present work).

TABLE 1: Parameters ϵ_j and τ_j and Variance of the Fit σ^2 Obtained from Fitting the Dielectric Spectrum of 0.363 M $MgSO_4$(aq) with Eq 2 Assuming $3 \leq n \leq 6$ Independent Dispersion Steps of the Debye (D) Type[a]

	$n=3$ 3D	$n=3$ 3D[b]	$n=4$ 4D	$n=5$ 4D	$n=5$ 5D	$n=6$ 6D
ϵ	87.25	84.64	96.91	87.05	87.05	97F
τ_1	440	129	6400	400F	400F	7400
ϵ_2	82.75	69.02	85.70	83.00	83.01	85.91
τ_2	113	8.52	153	127	126	266
ϵ_3	69.68	7.56	71.85	70.63	70.70	84.16
τ_3	8.38	1.5	22.6	16.2	20.8	141
ϵ_4			65.95	63.22	66.93	70.21
τ_4			7.94	7.79	8.16	24.4
ϵ_5					6.71	67.27
τ_5					1.52	8.16
ϵ_6						6.65
τ_6						1.43
ϵ_∞	6.27	4.49F	5.85	5.78	5.08	5.12
σ^2	0.078	0.191	0.049	0.061	0.059	0.049

[a] F indicates that the parameter was fixed (not adjusted) in the fitting procedure. Units: τ_j in 10^{-12} s. [b] Reference 23.

For this solution, the low-frequency contribution is rather symmetric (Figure 2), and it is also possible to obtain a reasonable fit with $n = 2$ using a superposition of a low-frequency Cole−Cole or Cole−Davidson equation and just one Debye equation for the ~20 GHz relaxation. However, the shape of this low-frequency shoulder is quite different at other concentrations (Figure 1b). These marked changes in shape with c cannot be fitted satisfactorily with *any* $n = 2$ model. Even for the 0.363 M solution, although the fits with $n = 2$ produce reasonably low σ^2 values of ~0.07, the distribution of errors is not random. Such fits deviate systematically from the observed spectrum below 0.6 GHz, at ~3 GHz, and above 40 GHz, suggesting that more than one relaxation process operates at both low and high frequencies. Thus, the low value of σ^2 obtained for the $n = 2$ models at $c = 0.363$ M is fortuitous.

A three-Debye-process (3D) model also fits the combined data well (Table 1, column 2) at $c = 0.363$ M but can be rejected on similar grounds to the $n = 2$ models. For comparison, column 3 of Table 1 shows the results obtained by Barthel et al.[23,24] at this concentration. The quality of their 3D fit is clearly far worse than the equivalent fit for the present data, reflecting the limitations in their low-frequency data, as discussed above.

Fitting the combined data at $c = 0.363$ M with $n \geq 4$ must also be done with care. Unrestrained 4D (column 4) and 5D (not shown) models (the unrestrained 6D model did not converge) suggest a contribution at ~0.025 GHz (with a relaxation time of ~7000 ps). Such a process is far outside our accessible frequency range nor is it "observed" at other concentrations. Thus, the small variance obtained for such fits is again not significant. On the other hand, at other concentrations, free-running fits with $n \geq 4$ clearly indicated the existence of a relaxation at ~0.5 GHz (Table 2). Thus, it appears reasonable to clamp one relaxation time at ~400 ps for the $c = 0.363$ M spectrum. From the various fits with the 4D, 5D, and 6D models, only the restrained 5D fit (column 6 of Table 1) yielded physically reasonable parameters (including the value of ϵ), with small σ^2 and no obvious systematic deviations. It is noteworthy that the fast water process at $\tau \approx 1.5$ ps is only recovered with fits using $n \geq 5$ equations.

Ultimately, it is the changes in the spectra at low frequencies with changing solute concentration (Figure 1) that enable the unambiguous identification of three solute-related processes in this system. At low c, the most significant process in the ϵ'' spectra is centered around 0.5 GHz. At $0.1 \leq c/\mathrm{M} \leq 0.7$, this

TABLE 2: Limiting Permittivities, ϵ_j, Relaxation Times, τ_j, and Variance of the Fits, σ^2, Obtained for the Dielectric Relaxation Spectra of $MgSO_4$(aq) at 25 °C[a]

c	ϵ	τ_1	ϵ_2	τ_2	ϵ_3	τ_3	ϵ_4	τ_4	ϵ_5	τ_5	ϵ_∞	σ^2
0	78.32		78.32		78.32		78.32	8.33	6.32	1.1	4.57	
0.01691	79.64	257	77.86		77.86		77.86	8.28	5.74	1.0F	4.60	0.074
0.02950	81.24	276	77.59		77.59	22.3	76.90	8.29	6.52	1.0F	5.03	0.058
0.05007	83.09	307	78.03	130	76.82	22.0F	76.79	8.29F	6.36			0.022
0.07296	84.69	315	78.55	129	76.30	23.4	74.04	8.03	6.12	1.0F	5.43	0.068
0.07744	84.77	324	78.62	113	75.82	22.0	75.37	8.21	6.16	1.0F	5.44	0.054
0.0998	85.92	412	81.19	156	75.58	16.2	74.80	8.25F	6.34			0.027
0.1498	87.27	408	82.45	151	74.63	18.4	72.62	8.21F	6.71			0.030
0.2001	88.31	500	83.74	147	73.61	19.6	71.35	8.13	6.12	1.0F	5.10	0.078
0.2706	88.36	421	83.27	135	72.42	25.8	69.93	8.14F	6.75			0.042
0.3634	87.05	400F	83.01	126	70.70	20.8	66.93	8.16	6.71	1.5	5.08	0.059
0.5002	86.08	295	81.90	131	69.65	29.1	64.42	8.01F	6.37			0.048
0.6472	83.77	300F	80.34	117	67.00	21.7	59.22	7.94	6.81	0.7	4.44	0.072
0.8206	80.91	286	78.52	119	64.90	22.4	55.10	7.89	7.13	1.0F	4.71	0.058
1.120	76.75	288	73.18	115	60.47	21.9	48.32	7.75	7.03	1.0F	4.04	0.070
1.351	76.09	311	69.25	117	59.34	26.6	47.25	7.74F	5.77			0.056
1.599	73.80	426	67.44	124	56.32	24.6	42.67	7.74	6.43			0.079
1.897	72.05	459	62.43	132	53.15	26.3	38.74	7.68F	5.78			0.048
2.236	70.92	499	57.18	122	48.87	23.2	32.37	7.66	6.96			0.061

[a] Parameters followed by the letter "F" were fixed (not adjusted) in the fitting procedure. Data for pure water were taken from ref 39. Units: c in mol L^{-1}; τ_j in 10^{-12} s.

feature is systematically replaced by another centered on 1 GHz. At still higher c, this is followed by an increase at ~9 GHz. Despite the broadness of the DRS loss peaks, such differences are easily distinguished. Above 1.2 M the dielectric loss at ~0.5 GHz rises again (this is unusual and will be discussed in detail in sections 4.3 and 4.6).

Generally, it was found that for the spectra covering $\nu_{min} \leq \nu/\text{GHz} \leq 89$ a sum of five Debye equations (the 5D model; $n = 5$ in eq 2; see Figure 2) gave the smallest value of σ^2. At low c, the amplitudes of some of the low-frequency processes become too small to be resolved, but the 5D model was the only one that yielded a self-consistent set of relaxation parameters that could be assigned to plausible microscopic processes over the whole concentration range. The parameters so obtained are summarized in Table 2 and shown in Figures 3−5 as filled symbols. To fit those spectra consisting of VNA data alone, which are not affected by the high-frequency side of the water relaxation, a 4D model was used for which the relaxation time of bulk water, $\tau_4(c)$, was fixed at values interpolated from the 5D model.

As can be seen from Table 2, the final 4D or 5D model, corresponding to three solute-related processes plus one (for $\nu \leq 20$ GHz spectra) or two (for $\nu \leq 89$ GHz spectra) solvent-related processes, gave a good fit to all of the present and previous[23,24] spectra. They also produced relaxation parameters and amplitudes that varied smoothly with changing solute concentration. This is a necessary but not sufficient condition for these fits to have physical significance. Decisive confirmation comes from being able to quantitatively relate the DRS parameters so obtained to information gathered using other techniques, as discussed below.

4. Results and Discussion

4.1. General Comments. Typical combined DR spectra featuring both the permittivity (in-phase) and loss (out-of-phase) responses over the frequency range $\nu_{min} \leq \nu/\text{GHz} \leq 89$ are given for $MgSO_4$(aq) in Figure 1. Clearly, there are very pronounced changes in the spectra from that observed for bulk water. The relaxation parameters obtained from these spectra are summarized in Table 2. Occasional addition of small amounts of acid established that the results were independent of pH, indicating that neither hydrolyzed species nor HSO_4^- contributed significantly to the observed spectra.

The major feature of the DR spectra of $MgSO_4$(aq), as is usual in aqueous electrolyte solutions,[25,39] is the process centered on ~8 ps (~20 GHz, Figure 2) that corresponds to the cooperative relaxation of the H-bond network in bulk water. In addition, there is a high-frequency process at ~1 ps, which is thought to be due to the reorientation of mobile water molecules[23,24,35−37,39] but which is barely detectable in the present spectra as a small shoulder at ~90 GHz. At $c > 1.1$ M, it was not possible to resolve this high-frequency process probably because it moved outside the range of the present apparatus, as has been observed for other concentrated aqueous electrolyte solutions.[38,40]

As discussed in section 3 above, the observed spectra are best accounted for by a model incorporating four or five Debye processes (Figures 1 and 2) consisting of the one or two higher frequency processes associated with bulk water and three solute-related processes at lower frequencies. The only previous detailed DRS study of $MgSO_4$(aq),[23,24] the data of which are incorporated in the present work, detected just one solute-related process. The failure to detect further processes, although their possible existence was recognized,[24] is a direct consequence of the relatively high value of ν_{min} (≥1 GHz) and the lower accuracy of the low-frequency data with the equipment then available.

One possible low-frequency process could result from the presence of "slow" (i.e., *partially* immobilized on the DR time scale) water molecules in the hydration spheres of free Mg^{2+} or SO_4^{2-} ions (or ion pairs). However, this is ruled out by the absence of any similar process in either $MgCl_2$(aq)[23] or Na_2SO_4(aq)[21] and because if such a model is assumed, it produces physically unrealistic hydration numbers for the counterion in each case. Of all other possible explanations of the three solute-related DR processes in $MgSO_4$(aq), the most plausible is that they arise from the presence of the three ion pair types (2SIP, SIP, and CIP), whose existence has long been inferred from the detection of three equilibrium processes by ultrasonic absorption measurements.[5−7] However, this is the first time that all three types of ion pairs have been directly detected in such solutions. This assignment produces physically meaningful parameters, over the whole concentration range, that can be

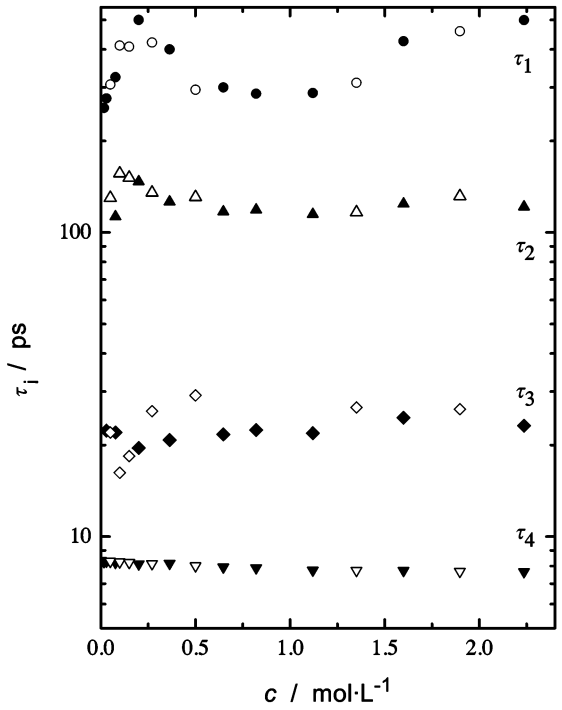

Figure 3. Measured relaxation times for processes 1−4 in $MgSO_4$(aq) at 25 °C obtained directly from wide-scan spectra (filled symbols), interpolated from wide-scan spectra (τ_4), or obtained from $\nu \leq 20$ GHz spectra (τ_1 to τ_3) with τ_4 fixed at the interpolated value (open symbols).

linked to information obtained with other methods. Other possible models do not.

4.2. Relaxation Times. As is usually observed for aqueous solutions of inorganic electrolytes,[40] the relaxation time for bulk water (τ_4) decreased slightly but smoothly with increasing solute concentration (Figure 3). This enabled τ_4 values to be interpolated reliably for those spectra recorded only at $\nu \leq 20$ GHz, which in turn allowed reasonable estimation of relaxation times (τ_1, τ_2, and τ_3) for the three slower processes from such spectra (open symbols in Figure 3). At low c, because of the very small amplitudes of these three processes, there are large uncertainties in the τ values that are reflected in the scatter of the data (Figure 3). Within the likely experimental error limits, τ_2 and τ_3 are independent of c. In contrast, τ_1 shows a small maximum at $c \approx 0.2$ M (which may be within the error limits) followed by a definite increase, from ca. 300 to 500 ps, at $c > 1$ M. The latter is unusual and will be discussed further below (sections 4.3 and 4.6).

The rotational correlation time, τ', of an ion pair may be estimated from its molecular volume, V_m, with the help of the Stokes−Einstein-Debye equation:

$$\tau' = \frac{3V_m f_\perp C}{k_B T}\eta \qquad (3)$$

where $f_\perp$ is a geometric factor that describes the ellipsoidal shape of the ion pair and C describes the hydrodynamic coupling between ion-pair rotation and solution viscosity ($C = 1$ for stick; $C = 1 - f_\perp^{-2/3}$ for slip). At $c \to 0$, it may be assumed that $\tau' \approx \tau$, and with the viscosity of the pure solvent $\eta = 0.890$ cP,[41] the approximate correlation times listed in Table 3 were obtained. The estimates of τ' for 2SIP, SIP, and CIP are consistent with the observed correlation times τ_j ($j = 1...3$). Exact agreement is not expected because experience shows that the experimental coupling parameter, C, is generally between the stick and slip limits.[19,31]

TABLE 3: Ion-Pair Dipole Moments and Rotational Correlation Times Calculated via Eq 3 at $c \to 0$ for CIP, SIP, and 2SIP[a]

ion pair	μ_{IP}	τ' stick	τ' slip	τ_1	τ_2	τ_3	A_i
CIP	28.6	73	5			∼22	0.266
SIP	55.7	174	35		∼115		0.188
2SIP	82.8	350	127	∼300			0.131

[a] Units: μ_{IP} in D (1D = 3.3356×10^{-30} C m); τ' and τ_j in 10^{-12} s.

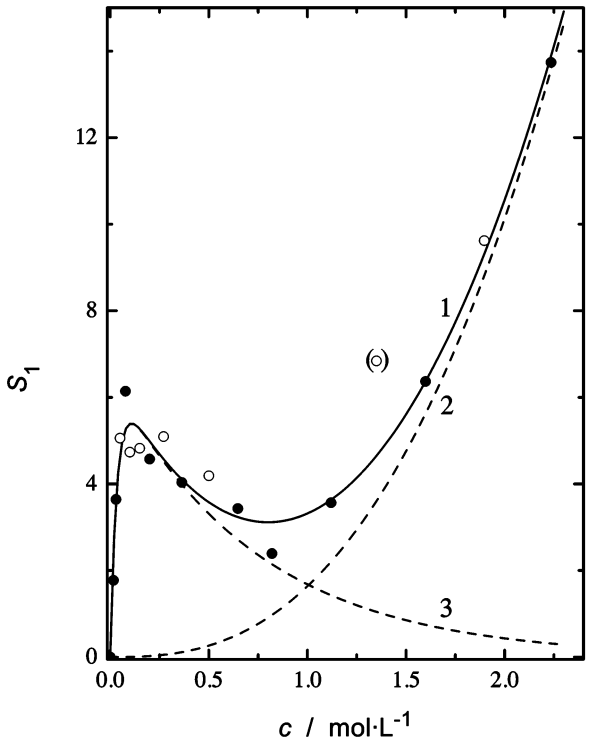

Figure 4. Amplitude of the slowest relaxation process, S_1, centered on ∼0.4 GHz, in $MgSO_4$(aq) at 25 °C: observed amplitude (1); "excess" amplitude (2); 2SIP contribution (3). Datum in parentheses is excluded.

4.3. Amplitudes of the Low-Frequency Processes. Process 1 is ascribed to the presence of 2SIPs, but its amplitude S_1 (Figure 4, curve 1) is anomalous. With increasing c, S_1 shows the expected[21,26] rapid increase followed by a decline, as the 2SIPs form and then begin to be replaced by SIPs and CIPs. However at $c > 1$ M, S_1 again *increases* dramatically. The probable origin of this effect is discussed in section 4.6, but for calculational purposes the amplitude of the first process was assumed to be a composite of a 2SIP contribution, S_{2SIP}, dominant at $c < 1$ M and consistent with those observed previously for Na_2SO_4(aq),[21] and another "excess" contribution, S_{EX}, that becomes significant only at higher c. That is,

$$S_1 = S_{2SIP} + S_{EX} \qquad (4)$$

For convenience, these two contributions (Figure 4, curves 2 and 3) can be described by a power law in c:

$$S_{2SIP} = a_0[\exp(-a_1 c) - \exp(-a_2 c)] \quad \text{and} \quad S_{EX} = a_3 c^{a_4} \qquad (5)$$

where a_i are empirical parameters. The amplitudes of the second and third processes, S_2 and S_3, are shown as functions of c in Figure 5. As would be expected, S_2, corresponding to the presence of SIPs, goes through a maximum while that for CIPs (S_3) increases steadily with c.

4.4. Quantitative Analysis of the Ion-Pairing Processes. The amplitudes S_{2SIP}, S_2, and S_3 were analyzed quantitatively

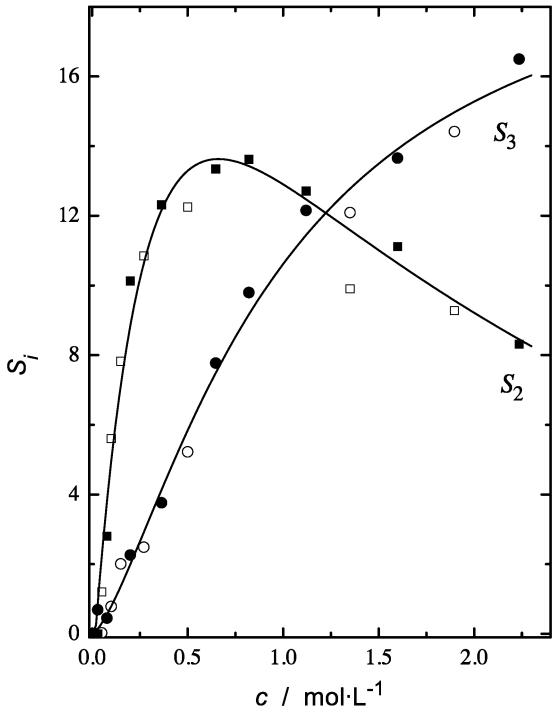

Figure 5. Amplitudes of the second and third processes in $MgSO_4$(aq) at 25 °C, corresponding to SIP (at ~1.3 GHz) and CIP (at ~10 GHz), respectively. Filled and open symbols are as defined in the caption of Figure 3.

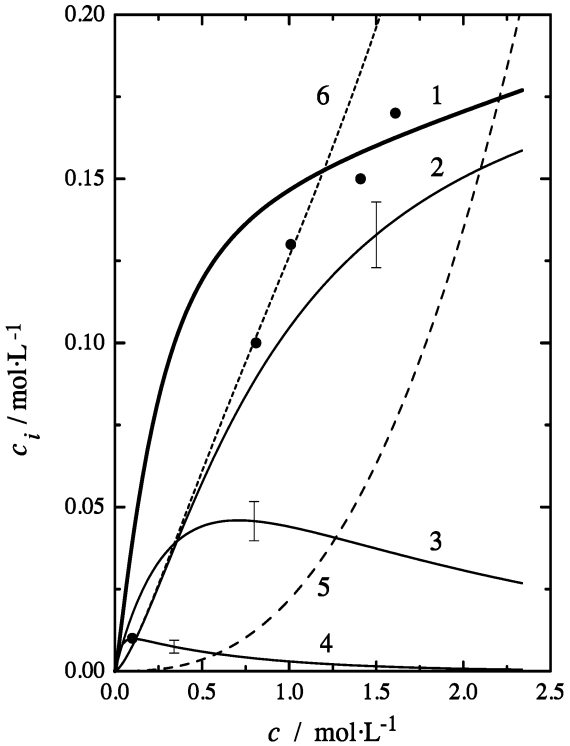

Figure 6. Species concentrations (c_i) in $MgSO_4$(aq) at 25 °C obtained from the present DRS data: total ion-pairs excluding "TI" (1); CIP (2); SIP (3); 2SIP (4); "TI" (5, long-dashed line); CIP + "TI" (6, short-dashed line). Filled symbols were calculated from the Raman data of ref 43.

employing the procedure outlined in detail elsewhere.[21,24,26] In essence, this involves using the modified Cavell equation:[24,42]

$$c_i = \frac{3(\epsilon + (1-\epsilon)A_i)}{\epsilon} \frac{k_B T \epsilon_0}{N_A} \frac{(1-\alpha_i f_i)^2}{g_i \mu_i^2} S_i \qquad (6)$$

where ϵ_0, k_B, and N_A are, respectively, the permittivity of free space, Boltzmann's constant, and Avogadro's number; α_i, f_i, g_i, and μ_i are the polarizability, field factor, dipole correlation factor (for ion pairs, $g_i = 1$), and dipole moment of the species i; A_i is a geometric factor;[21,33] and T is the (Kelvin) temperature. Ion pairs were assumed to be ellipsoids with semiprincipal axes $a = r_+ + r_- + nr(H_2O)$, with $n = 0$, 1, 2; $b = c = r_-$; and polarizability $\alpha_{IP} = \alpha_+ + \alpha_- + n\alpha(H_2O)$. For $MgSO_4$(aq), $r_+ = 78$ pm, $r_- = 258$ pm, and $r(H_2O) = 142.5$ pm are the radii and $\alpha_+ = -0.28$ Å^3, $\alpha_- = 5.47$ Å^3, and $\alpha(H_2O) = 1.45$ Å^3 are the polarizabilities of the cation, the anion, and water, respectively.[41] The values required for the evaluation of eq 6 are given in Table 3 or are easily calculated using the relevant equations in Buchner et al.[21] The ion pair concentrations derived in this manner are given as a function of c in Figure 6.

As required by the presence of multiple stepwise equilibria, Scheme I, the 2SIP and SIP concentrations go through a maximum, at ~0.1 and ~0.6 M respectively, while the CIP concentration increases steadily with c. Also included in Figure 6 are the CIP concentrations calculated from the Raman data of Davis and Oliver[43] by assuming that only CIPs are detected by Raman spectroscopy (via the mode centered on ~993 cm^{-1}). The agreement is virtually quantitative up to $c \approx 1$ M. Note that the data of Davis and Oliver were chosen for this comparison because they have also shown that their CIP concentrations are consistent with those derived from the ultrasonic absorption measurements of Atkinson and Petrucci.[7] Clearly, all three techniques are in substantive agreement with respect to the existence *and* concentration of CIPs in $MgSO_4$(aq) at $c \leq 1$ M. The situation at $c > 1$ M is considered further below.

The species distribution, which can be calculated from the concentrations in Figure 6, varies considerably with c. Thus, the overall extent of ion-pairing in $MgSO_4$(aq) rises rapidly to a maximum of ~40% (~14% 2SIP, ~18% SIP, ~ 8% CIP) at $c \approx 0.1$ M but then decreases monotonically to ~8% (~1% SIP, ~7% CIP) as c approaches saturation. This effect, which has been termed "redissociation", reflects the decline in the overall association constant with increasing ionic strength, I.

The equilibrium constants for the individual steps in Scheme I, expressed as concentration ratios and calculated from the ion pair concentrations obtained from the experimental amplitudes via eq 3, are summarized in Figure 7. The values of $K_1 = [2SIP]/([Mg^{2+}][SO_4^{2-}])$ for the initial association of the fully hydrated ions to form 2SIPs (where the square brackets denote concentrations) show the marked decrease with c (or I) expected for an equilibrium between highly charged ions.[1,4] On the other hand $K_2 = [SIP]/[2SIP]$ and $K_3 = [CIP]/[SIP]$, which relate to equilibria that involve only a loss of water, show small variations with c. The somewhat larger decrease at $c \lesssim 0.5$ M shown by both K_2 and K_3 appears to be real in that the (extrapolated) infinite dilution values are in good agreement (Figure 7) with those obtained at low I (corrected to infinite dilution) from the ultrasonic absorption measurements.[5-7] These decreases may reflect changes in activity coefficients (and thus water activity), which are appreciable in $MgSO_4$(aq) solutions.[12] It will be shown below that although the total water concentration (but not its activity) is essentially constant, the apparent concentration of "free" bulk water, derived from the water dispersion amplitudes ($S_4 + S_5$), decreases considerably with increasing solute concentrations. Since the equilibria corresponding to K_2 and K_3 both involve the release of water, Scheme I, this effect

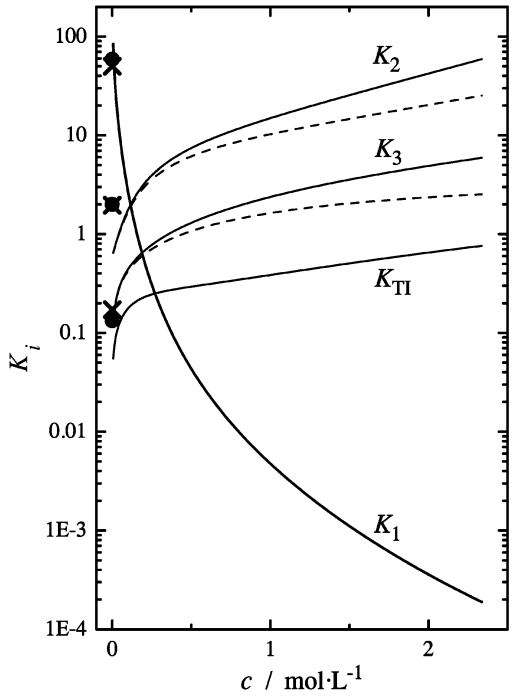

Figure 7. Equilibrium constants for the formation of individual species in $MgSO_4$(aq) at 25 °C obtained from the present DRS measurements. K_1, K_2, K_3 are as defined in Scheme I, and K_{TI} is as defined by Scheme II). For K_2 and K_3: with (dashed lines) and without (solid lines) inclusion of bulk water concentration factor (see text). Symbols: estimates of K_1, K_2, and K_3 at infinite dilution from the ultrasonic studies of ref 6 (●) and ref 7 (×).

should be allowed for: $K_n(\text{corr}) = K_n c_s^{ap}(c)/c_s^{bulk}(0)$. The corrected K_n values exhibit a significantly smaller dependence on I (dashed lines in Figure 7).

It is readily shown[21] that the overall stability constant K_A is related to the stepwise constants via

$$K_A = K_1 + K_1K_2 + K_1K_2K_3 \tag{7}$$

The values of K_A calculated directly from the experimental amplitudes are plotted in Figure 8 as a function of I (corrected for ion association). For convenience, these values were fitted to a Guggenheim-type function:

$$\log K_A = \log K_A^\circ - \frac{2A_{DH}|z_+z_-|\sqrt{I}}{1+\sqrt{I}} + B_K I + C_K I^{3/2} \tag{8}$$

where A_{DH} is the Debye−Hückel parameter for activity coefficients of electrolytes in water[1] and B_K and C_K are empirical constants. The log K_A values were adequately fitted without the need for the term in $I^{3/2}$ usually required[21] for such data, i.e., $C_K = 0$. The standard state (infinite dilution) value so obtained, $K_A^\circ = 167 \pm 11$, is in excellent agreement with the value $K_A^\circ = 157 \pm 3$ recently reported by Tomšič et al.[14,44] from high precision conductivity measurements and well within the spread of reliable literature values.[12,45]

In this context, it is important to recognize that the equilibrium constant obtained from Raman spectroscopy is *not directly comparable* with any of the stepwise constants (K_i values, including K_3) derived by DRS or ultrasonic absorption, or with the overall association constant (K_A) obtained from traditional thermodynamic and conductance measurements. Instead, Raman spectroscopy utilizing ligand vibrations measures a constant that describes the equilibrium between the Raman-indistinguishable concentrations of {free ions + 2SIP + SIP} and the Raman-detected CIP. The 'apparent' constant obtained by Raman spectroscopy is always significantly (and sometimes very much) smaller than the overall constant. The exact mathematical relationship between the Raman-determined constant K_A^R and K_i is discussed in detail elsewhere.[46] Failure to understand this situation has been the source of a great deal of confusion in the literature and has misled many authors[12,19] into believing that the uncertainties in the association constants are much greater than they actually are.

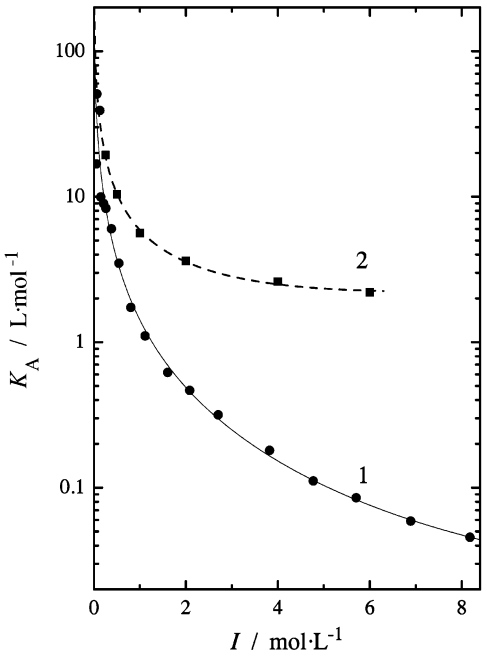

Figure 8. Overall ion-pairing constant (K_A) for $MgSO_4^0$(aq) as a function of the ionic strength at 25 °C in various media: present DRS values in $MgSO_4$ (1); potentiometric data of ref 45 in CsCl (2). Lines are Guggenheim-type, eq 8, fits to the data.

It is interesting to compare the overall K_A values at finite I derived from the present DRS results with those obtained in the only other systematic investigation of the dependence of K_A on I: the potentiometric study of Kratsis et al.[45] in CsCl media. Although showing a broadly similar value of K_A° (the measurements of Kratsis et al. were not designed to determine this quantity, being restricted to $I \geq 0.25$), the values of K_A and their trend with I (Figure 8, curve 2) differ from the present results. Such an effect has been observed previously for $K_A(NaSO_4^-)$[21] and is almost certainly a reflection of differences in activity coefficients, since there is a considerable difference in the "self-medium" of a concentrated 2:2 electrolyte, as employed in the present DRS measurements, and the same species interacting at more or less trace levels in a medium containing a vast excess of an indifferent (noninteracting) 1:1 electrolyte.

4.5. Hydration Numbers. Effective hydration numbers can be obtained from DRS data as outlined in detail elsewhere.[21,25] In essence this involves calculation of the apparent water concentration c_s^{ap} in the electrolyte solutions using the solvent-normalized Cavell equation:

$$c_s^{ap}(c) = g_s(c)\frac{c_s^{bulk}(c)}{g_s(0)} = c_s(0)\frac{S_s^{eq}(c)}{S_s(0)}\frac{2\epsilon(c)+1}{\epsilon(c)}\frac{\epsilon_s}{2\epsilon_s+1} \tag{9}$$

where the subscript s denotes the solvent value.

Note that the concentration of (unperturbed) bulk water in a solution, $c_s^{bulk}(c)$, cannot be measured directly because of

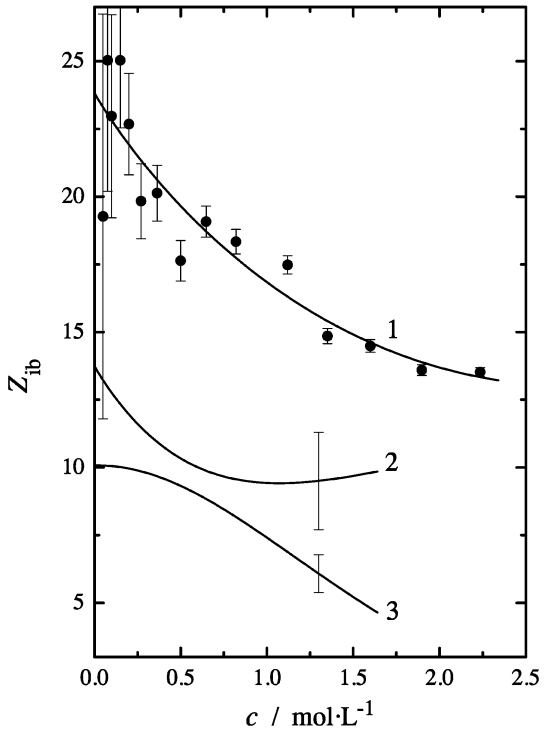

Figure 9. Effective solvation numbers, Z_{ib}, of $MgSO_4$(aq) at 25 °C assuming "slip" boundary conditions for the kinetic depolarization effect: total (1); Mg^{2+} (2); SO_4^{2-} (3, from ref 21).

possible changes in the dipole correlation factor $g_s(c)$ with c. The equilibrium amplitude of the solvent dispersion in the electrolyte solutions, $S_s^{eq}(c)$, is given by

$$S_s^{eq}(c) = S_s(c) + \Delta_{kd}\epsilon(c) \tag{10}$$

where $\Delta_{kd}\epsilon(c)$ represents the dynamic "kinetic depolarization" contribution to the observed amplitude, associated with the movement (transport) of ions in the electric field.

The amplitude of nonbound water, $S_s(c)$, was measured as $\epsilon_4(c) - \epsilon_\infty(0)$, where $\epsilon_\infty(0) = 4.57$ was taken as that given for pure water by Buchner et al.[39] This value differs slightly from those obtained from fitting the present spectra (Table 2) but is preferred because it is based not only on DRS data but also on far-IR measurements, which are better able to define the very fast water process (process 5 in the present spectra) and thus provide a more reliable estimate of $\epsilon_\infty(0)$.[47] Effective hydration numbers, expressed as the number of "irrotationally bound" water molecules, Z_{ib}, were then calculated with allowance for $\Delta_{kd}\epsilon(c)$, assuming "slip" boundary conditions for the ions,[21,25] via

$$Z_{ib} = (c_s - c_s^{ap})/c \tag{11}$$

where c_s is the stoicheometric concentration of water in the solution.

The values so obtained are presented in Figure 9 and show that the hydration number of $MgSO_4$ decreases from ~24 at infinite dilution to ~15 at high concentrations. These values are broadly consistent with the figure of ~20 estimated by Malatesta and Zamboni[19] from membrane potential measurements. The *ionic* hydration numbers (Figure 9) were obtained by assuming $Z_{ib}(SO_4^{2-})$ to be the same as those determined in Na_2SO_4(aq).[21] These quantities are based ultimately on the assumption that $Z_{ib}(Cl^-) = 0$ in NaCl(aq),[25] which has been shown to produce a consistent set of hydration numbers for the alkali metal ions that are in agreement with molecular dynamics simulations.[40]

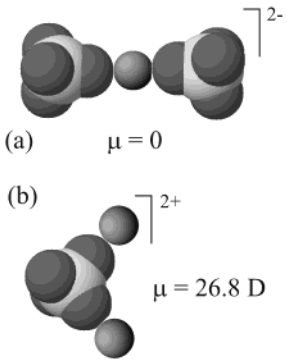

Figure 10. Probable structures of the triple ions formed in $MgSO_4$-(aq) solutions, with water molecules omitted for clarity: $Mg(SO_4)_2^{2-}$(aq), $\mu = 0$, assuming trans substitution of two SO_4^{2-} ions on an octahedral Mg^{2+} (a); $Mg_2SO_4^{2+}$(aq), $\mu = 26.8$ D, with two Mg^{2+} ions bound to a tetrahedral SO_4^{2-} (b).

The present values of $Z_{ib}(Mg^{2+})$ decrease from ~14 at infinite dilution to ~10 at high c (Figure 9), which is again consistent with the values estimated by Malatesta and Zamboni.[19] Scattering studies indicate a coordination number of 6 for Mg^{2+} in a variety of salt solutions,[48] but this refers only to the number of nearest neighbors, i.e., the primary hydration shell. Simulation studies using a combined quantum mechanical/molecular dynamics approach[49] confirm a coordination number of 6 but also indicate the presence of a significant second hydration shell containing about 12 water molecules, giving (at infinite dilution) a total hydration number of ~18. Similar findings were made in the earlier molecular dynamics simulations of Guàrdia et al.[50] and by Pye and Rudolph[16] using ab initio calculations. This level of agreement between the simulations and the present DRS estimates is encouraging; exact agreement would not be expected because the latter detects only those water molecules that are effectively "frozen" on the DR time scale.

4.6. "Excess" Amplitude. The "excess" amplitude, i.e., the unexpected increase in S_1 at $c > 1$ M (Figure 4), cannot be assigned to 2SIPs because an increase in the 2SIP concentration with decreasing water content is illogical and would violate Le Chatelier's principle. The most plausible explanation of this effect is the existence of one (or more) additional dipolar species. Since the increase in S_1 occurs only at high concentrations, it seems reasonable to ascribe it to a "higher order" complex such as a triple or, less likely, quadruple ion species. Alternatively, molten-salt-like collective oscillations may be occurring.[29,47,51,52]

The existence of higher order ion aggregates has previously been invoked to account for the thermodynamic properties of concentrated $MgSO_4$(aq).[2,53,54] However, in the absence of independent evidence, such species have generally been regarded as little more than mathematical conveniences because, as already noted, it is possible to model the thermodynamic behavior of these solutions without invoking any complexes at all.[12,19,55]

Statistical considerations suggest that, as well as the three types of 1:1 ion pairs (2SIP, SIP, and CIP), the most likely additional species present in $MgSO_4$(aq) are the triple ions $Mg(SO_4)_2^{2-}$(aq) and $Mg_2SO_4^{2+}$(aq). Because such species appear to form only at high electrolyte concentrations, it seems reasonable to assume that they are contact (inner sphere) species. The probable structures of these two triple ions are shown in Figure 10.

With respect to $Mg(SO_4)_2^{2-}$(aq), electrostatic and steric considerations make it probable that this species would form

via trans substitution of water molecules in the first coordination shell of the octahedral aquated Mg^{2+} ion by the two SO_4^{2-} ions. Such a symmetrical species would not be dipolar (i.e., $\mu = 0$) and would not therefore be seen in the DR spectrum. In contrast, $Mg_2SO_4^{2+}$(aq), in which the two Mg^{2+} ions are bound to the tetrahedral SO_4^{2-} ion, is essentially V-shaped and thus must be dipolar. Following the procedure outlined by Barthel et al.[24] for the calculation of dipole moments of charged ion pairs and assuming the center of mass as the pivot, the dipole moment of $Mg_2SO_4^{2+}$, μ_{TI}, is estimated to be 26.8 D. This $Mg_2SO_4^{2+}$(aq) triple ion is proposed as the source of the "excess" amplitude observed at low frequencies and high concentrations. Note that this does not mean that it forms in preference to, or even to the same extent as, $Mg(SO_4)_2^{2-}$(aq) in concentrated $MgSO_4$(aq) solutions but merely that of the two possible TIs, only $Mg_2SO_4^{2+}$(aq) will be *detectable* by DRS.

It is apposite to note here that the existence of TIs (or any other higher aggregate) cannot alone explain the dependence of S_1 on c (Figure 4, curve 1) because such species will exist in negligible amounts at low c. As noted in section 4.3, for analogous reasons the presence of 2SIPs alone is also inconsistent with the observed S_1 values. The existence of *both* species (over different ranges of c) is required to account for the observations.

The equilibrium that produces the triple ion $Mg_2SO_4^{2+}$(aq), TI, can be written as

$$\mathrm{CIP} + \mathrm{Mg}^{2+} \overset{K_{TI}}{\Leftrightarrow} \mathrm{TI} \qquad \text{(II)}$$

The resulting triple-ion concentrations, c_{TI} (curve 5), calculated from the modified Cavell equation, eq 6, using the estimated dipole moment ($\mu = 26.8$ D), and the total concentration of inner sphere species, $c_{CIP} + c_{TI}$ (curve 6), are included in Figure 6.

The simultaneous existence of CIPs and TIs in $MgSO_4$(aq) is in principle feasible up to the saturation limit. At $c = 1$ M the average distance between two ions is 940 pm or $2.8(r_+ + r_-)$; at 2 M it is $2.2(r_+ + r_-)$. Thus, the average distance *between* anions and cations is $\sim 4r(H_2O)$ at 1 M, $\sim 3r(H_2O)$ at 2 M, and $\sim 2.4r(H_2O)$ at 2.5 M. Because of ion association, the average distance of "free" ions will be slightly larger but not by much. Obviously, stable 2SIPs are practically impossible at $c > 1$ M because other ions will be at a distance similar to the charge separation in the ion pair. SIPs are conceivable up to saturation but must become unfavorable relative to CIPs and TIs. The high density of ions implies strong interactions between any type of aggregate (IPs, TIs, etc.) and its surroundings. This may explain the large relaxation time ($\sim$400 ps) observed for the TI; from eq 3 one would only expect 100 ps for stick limits (and less for slip).

4.7. Raman Spectroscopy. Raman spectra of $MgSO_4$(aq) solutions have been studied on numerous occasions.[16,17,43] It is well established that, in addition to the strong $\nu(a_1)$ band corresponding to free SO_4^{2-}(aq) ions at $\sim$983 cm^{-1}, a shoulder whose intensity increases with increasing c appears at $\sim$993 cm^{-1}. Although there has been some controversy about the origin of this new mode,[56] it is most reasonably assigned to the formation of a CIP.[16,17,43,46] This assignment is supported by the careful studies of Rudolph and co-workers[16,17] who have detected the required changes in the very weak, low-energy $Mg-OH_2$ and $M-O-SO_3$ bands in addition to the 993 cm^{-1} mode. These observations have recently been confirmed using a more sensitive spectrometer, and it has been shown conclusively[46] that the observed changes are entirely consistent with ion pairing. Furthermore, quantitative correlations between the various Raman spectral changes associated with the formation of the CIP and with the present DRS data have been demonstrated.[46]

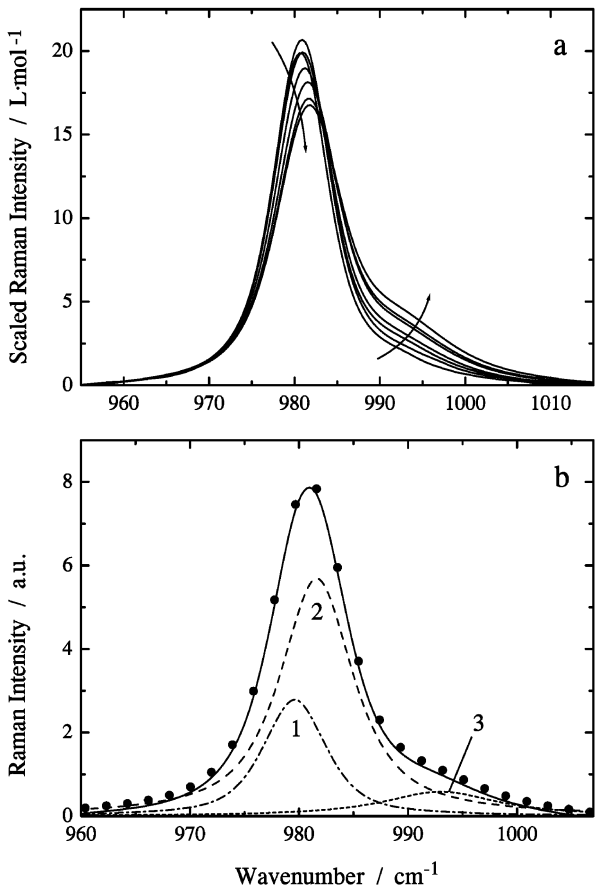

Figure 11. Concentration-normalized Raman spectra in the $\nu(a_1)$ region of $MgSO_4$(aq) at 25 °C. (a) At c/M = 0.1, 0.4, 0.8, 1.6, 2.0, 2.5: increasing in the direction of the arrows. (b) Approximate decomposition of an observed Raman spectrum at $c = 0.40$ M: observed intensity (symbols); calculated spectrum (full line); {free SO_4^{2-} + 2SIP} (1); SIP (2); CIP (3). Note that the decomposition is indicative only. Whereas peak positions are reasonable, intensities are not. More accurate spectra and decompositions are given elsewhere.[46]

Measurements of the Raman spectra of $MgSO_4$(aq) focusing on the $\nu(a_1)$ band profile (950−1050 cm^{-1}) are shown in Figure 11a. The spectra are virtually identical with those reported by Rudolph et al.,[16,17,46] with the shoulder at $\sim$993 cm^{-1} corresponding to the presence of CIPs being readily apparent. Interestingly, very small but systematic variations with increasing c in the position and symmetry of the main peak at $\sim$983 cm^{-1} were noted. Although it is generally thought that ligand-based vibrations are influenced only by the presence of CIPs,[15] the most straightforward explanation of these effects is to ascribe them to SIPs (it seems reasonable to continue to assume that 2SIP would be indistinguishable from free SO_4^{2-}(aq)). Uncertainties in the measurements, especially with respect to resolution and baseline corrections and the small magnitude of the changes, precluded a quantitative analysis of this aspect of the present spectra. An approximate decomposition is shown in Figure 11b; the variations of the spectral components with c were qualitatively (though not quantitatively) consistent with this interpretation. More importantly, the existence of this easily overlooked effect has now been confirmed.[46] By use of a more accurate spectrometer and more sophisticated processing techniques, the band decompositions obtained by Raman spectros-

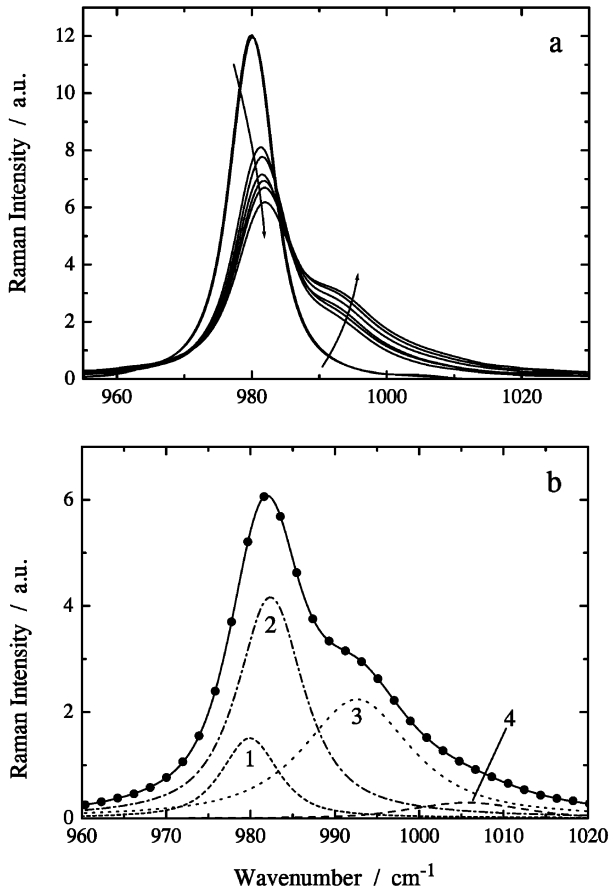

Figure 12. Raman spectra in the $\nu(a_1)$ region for solutions containing 0.5 M $(NH_4)_2SO_4$ + x M $MgCl_2$ at 25 °C. (a) At x/M = 0, 1.5, 1.75, 2.0, 2.25, 2.5, 2.75: increasing in the direction of the arrows. (b) Approximate decomposition of an observed Raman spectrum, x = 2.80 M: observed intensity (symbols); calculated spectrum (full line); {free SO_4^{2-} + 2SIP} (1); SIP (2); CIP (3); possible TI (4). Note that the decomposition is indicative only. Whereas peak positions are reasonable, intensities are not. More accurate spectra and decompositions are given elsewhere.[46]

copy[46] have been shown to be in *quantitative* agreement with the present DRS results.

As is customary in Raman spectroscopy, $MgSO_4$(aq) spectra reported to date have been made on the salt solutions themselves, i.e., at a fixed Mg^{2+}/SO_4^{2-} ratio. To better explore the possible formation of other species, it is useful to investigate spectra generated under other conditions. Figure 12a shows the Raman spectra recorded in the $\nu(a_1)$ region when $MgCl_2$ ($\leq$2.75 M) is added to a fixed concentration (0.5 M) of $(NH_4)_2SO_4$. The major features at ~983 and ~993 cm^{-1} again predominate, with small systematic variations similar to those described above again being apparent in the ~983 cm^{-1} peak. More noteworthy, however, is the appearance of a fourth, very weak band at ~1007 cm^{-1}. Measurements (not shown) of spectra under other conditions produced similar results.[27] An approximate decomposition of the $\nu_1(a_1)$ envelope for these spectra is given in Figure 12b. A band in this position has recently been reported by Zhang and Chan[29,52] in their Raman studies of highly supersaturated droplets. They ascribed this band to triple ions, other possible higher order species, collective oscillations, or, less plausibly, chelated species.

Thus, although some of the effects are small, Raman spectroscopy performed with sufficient care under appropriate conditions yields data that are fully consistent with our interpretation of the present DRS measurements.[46]

4.8. Implications. The present DRS results, supplemented by Raman spectroscopy and consistent with earlier ultrasonic absorption studies, have shown unequivocally that $MgSO_4$(aq), an apparently "simple" higher-valent and largely dissociated electrolyte, is in fact a complex mixture of chemical species whose nature and relative concentrations vary considerably as a function of the overall solute concentration. The occurrence of the various types of ion pairs, and possibly other higher order species, in $MgSO_4$(aq) has implications for virtually all concentrated higher-valent electrolyte solutions.

First, it provides a straightforward explanation of the phenomenon of electrolyte "redissociation":[57] a direct consequence of the stepwise formation of the various types of ion pairs and the dependence of their formation constants on concentration (or ionic strength). Second, it provides a rationale for the difficulties that have been experienced in developing fundamental (nonempirical) models to describe the observed behavior of higher-charged electrolyte solutions. It is beyond the scope of this paper to address this problem, but it is hardly surprising that theories that have been largely designed to explain the properties of solutions on the basis of the presence of two or three solute species (i.e., two ions and a "complex") are not satisfactory. It is hard not to view theories that do not take into account the actual species present and their variation with the overall electrolyte concentration, however successful they may be for *correlating* known properties, as little more than exercises in numerology. It is inevitable that such theories will ultimately have to rely on significant numbers of empirical parameters.

Acknowledgment. The authors thank Prof. W. Kunz for the provision of laboratory facilities at Regensburg, Dr. W. W. Rudolph for providing us with material prior to publication and helpful discussions, and Dr. R. Neueder for assistance with the ELDAR database.

References and Notes

(1) Robinson, R. A.; Stokes, R. H. *Electrolyte Solutions*, 2nd ed.; Butterworth: London, 1970.
(2) Corti, H. R.; Fernandez-Prini, R. *J. Chem. Soc., Faraday Trans. 2* **1986**, *82*, 921.
(3) Pitzer, K. S., Ed. *Activity Coefficients in Electrolyte Solutions*, 2nd ed.; CRC Press: Boca Raton, FL, 1991.
(4) Barthel, J.; Krienke, H.; Kunz, W. *Physical Chemistry of Electrolyte Solutions*; Springer: Berlin, 1998.
(5) Eigen, M.; Tamm, K. *Z. Elektrochem.* **1962**, *66*, 93.
(6) Eigen, M.; Tamm, K. *Z. Elektrochem.* **1962**, *66*, 107.
(7) Atkinson, G.; Petrucci, S. *J. Phys. Chem.* **1966**, *70*, 3122.
(8) Berthon, G., Ed. *Handbook of Metal−Ligand Interactions*; Dekker: New York, 1995.
(9) Gianguzza, A., Pelizzetti, E., Sammartano, S., Eds. *Chemistry of Marine Water and Sediments*; Springer: Berlin, 2002.
(10) Whiting, B. I.; Muir, D. M. *Miner. Process. Extr. Metall. Rev.* **2000**, *21*, 527.
(11) See, for example, the following. Tikanen, A. C.; Fawcett, W. R. *Ber. Bunsen-Ges. Phys. Chem.* **1996**, *100*, 634.
(12) Rard, J. A. *J. Chem. Thermodyn.* **1997**, *29*, 533.
(13) Wachter, R.; Riederer, K. *Pure Appl. Chem.* **1981**, *53*, 1301.
(14) Tomšič, M.; Bester-Rogač, M.; Jamnik, A.; Neueder, R.; Barthel, J. *J. Solution Chem.* **2002**, *31*, 19.
(15) Brooker, M. H. Raman Spectroscopic Measurements of Ion Hydration. In *The Chemical Physics of Ion Hydration*; Dogonadze, R. R., et al., Eds.; Elsevier: Amsterdam, 1986; Part B, Chapter 4.
(16) Pye, C. C.; Rudolph, W. W. *J. Phys. Chem. A* **1998**, *102*, 9933.
(17) Rudolph, W. W.; Mason, R. *J. Solution Chem.* **2001**, *30*, 527.
(18) Tobe, M. L.; Burgess, J. *Inorganic Reaction Mechanisms*; Longman: Harlow, U.K., 1999.
(19) Malatesta, F.; Zamboni, R. *J. Solution Chem.* **1997**, *26*, 791.
(20) Buchner, R.; Barthel, J. *Annu. Rep. Prog. Chem. C* **2001**, *97*, 349.
(21) Buchner, R.; Capewell, S. G.; Hefter, G. T.; May, P. M. *J. Phys. Chem. B* **1999**, *103*, 1185.
(22) Pottel, R. *Ber. Bunsen-Ges. Phys. Chem.* **1965**, *69*, 363.

(23) Barthel, J.; Hetzenauer, H.; Buchner, R. *Ber. Bunsen-Ges. Phys. Chem.* **1992**, *96*, 988.
(24) Barthel, J.; Hetzenauer, H.; Buchner, R. *Ber. Bunsen-Ges. Phys. Chem.* **1992**, *96*, 1424.
(25) Buchner, R.; Hefter, G. T.; May, P. M. *J. Phys. Chem. A* **1999**, *103*, 1.
(26) Capewell, S. G.; Buchner, R.; Hefter, G. T.; May, P. M. *Phys. Chem. Chem. Phys.* **1999**, *1*, 1933.
(27) Chen, T. Ph.D. Thesis, Murdoch University, Perth, Australia, 2003.
(28) Riley, J. P.; Skirrow, G. *Chemical Oceanography*; Academic Press: London, 1975.
(29) Zhang, Y.-H.; Chan, C. K. *J. Phys. Chem. A* **2002**, *106*, 285.
(30) Barthel, J.; Popp, H. *J. Chem. Inf. Comput. Sci.* **1991**, *31*, 107.
(31) Barthel, J.; Bachhuber, K.; Buchner, R.; Hetzenauer, H.; Kleebauer, M. *Ber. Bunsen-Ges. Phys. Chem.* **1991**, *95*, 853.
(32) Barthel, J.; Buchner, R.; Eberspächer, P. N.; Münsterer, M.; Stauber, J.; Wurm P. *J. Mol. Liq.* **1998**, *78*, 82.
(33) Böttcher, C. F. J.; Bordewijk, P. *Theory of Electric Polarization*; Elsevier: Amsterdam, 1978; Vol. 2.
(34) Barthel, J.; Buchner, R.; Bachhuber, K.; Hetzenauer, H.; Kleebauer, M.; Ortmeier, H. *Pure Appl. Chem.* **1990**, *62*, 2287.
(35) Barthel, J.; Bachhuber, K.; Buchner, R.; Hetzenauer, H. *Chem. Phys. Lett.* **1990**, *165*, 369.
(36) Thrane, L.; Jacobsen, R. H.; Uhd Jepsen, P.; Keiding, S. R. *Chem. Phys. Lett.* **1995**, *240*, 330.
(37) Rønne, C.; Thrane, L.; Åstrand, P.-O.; Wallqvist, A.; Mikkelsen, K. V.; Keiding, S. *J. Chem. Phys.* **1997**, *107*, 5319.
(38) Buchner, R.; Barthel, J.; Gill, B. *Phys. Chem. Chem. Phys.* **1999**, *1*, 105.
(39) Buchner, R.; Barthel, J.; Stauber, J. *Chem. Phys. Lett.* **1999**, *306*, 57.
(40) Chen, T.; Hefter, G. T.; Buchner, R. *J. Phys. Chem. A* **2003**, *106*, 4025.
(41) Marcus, Y. *Ion Properties*; Dekker: New York, 1997.
(42) Cavell, E. A. S.; Knight, P. C.; Sheikh, M. A. *J. Chem. Soc., Faraday Trans.* **1971**, *67*, 2225.
(43) Davis, A. R.; Oliver, B. G. *J. Phys. Chem.* **1973**, *77*, 1315.
(44) Neueder, R. Personal communication.
(45) Kratsis, S.; Hefter, G. T.; May, P. M. *J. Solution Chem.* **2001**, *30*, 19.
(46) Rudolph, W. W.; Irmer, G.; Hefter, G. T. *Phys. Chem. Chem. Phys.* **2003**, *5*, 5253.
(47) Buchner, R.; Hölzl, C.; Stauber, J.; Barthel, J. *Phys. Chem. Chem. Phys.* **2002**, *4*, 2169.
(48) Neilson, G. W.; Tromp, R. H. *Annu. Rep. Prog. Chem. C* **1991**, *88*, 142.
(49) Tongraar, A.; Rode, B. M. *Chem. Phys. Lett.* **2001**, *346*, 485.
(50) Guàrdia, E.; Sesé, G.; Padró, J. A.; Kalko, S. G. *J. Solution Chem.* **1999**, *28*, 1113.
(51) Badiali, J. P.; Cachet, H.; Lestrade, J. C. *Ber. Bunsen-Ges. Phys. Chem.* **1971**, *75*, 297.
(52) Zhang, Y.-H.; Chan, C. K. *J. Phys. Chem. A* **2000**, *104*, 9191.
(53) Gardner, A. W.; Glueckauf, E. *Proc. R. Soc. London* **1969**, *A313*, 131.
(54) Archer, D. G.; Wood, R. H. *J. Solution Chem.* **1985**, *14*, 757.
(55) Rard, J. A.; Miller, D. G. *J. Chem. Eng. Data* **1981**, *26*, 33.
(56) Myneni, S. C. B. *Rev. Mineral. Geochem.* **2000**, *40*, 113.
(57) Friedman, H. L. *Annu. Rev. Phys. Chem.* **1961**, *12*, 171.